Ocean Engineering 287 (2023) 115899

Contents lists available at ScienceDirect

Ocean Engineering

journal homepage: www.elsevier.com/locate/oceaneng

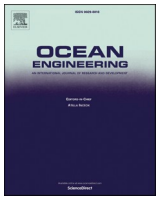

Impact of steel grade on a ship colliding with an offshore wind turbine monopile supporting structure

Karol Niklas [a,*], Alicja Bera [a], Yordan Garbatov [b]

[a] Gdansk University of Technology, Faculty of Mechanical Engineering and Ship Technology, Narutowicza 11/12, 80-233, Gdansk, Poland
[b] Centre for Marine Technology and Ocean Engineering, Instituto Superior Técnico, Avenida Rovisco Pais, 1049-001, Lisboa, Portugal

ARTICLE INFO

Handling Editor: Prof. A.I. Incecik

Keywords:
Large monopile
Ship
Collision
OWT
Steel grade
Material
Transition piece

ABSTRACT

Offshore wind power is experiencing rapid development around the world. The number of installations and their size is growing. Thousands of monopile support structures with diameters of 10 m and weights of 2000 tons will be installed in the coming years. Offshore wind power installations, often located close to the shore and shipping routes, pose a new challenge to ship safety. The study analyses the damages from an accidental collision between a 6500-tonne displacement Supply Offshore Vessel and the monopile support structure with a 10 m diameter and a 15 MW wind turbine. The head-on collision cases are performed according to the DNV-ST-0126, showing the consequences for the ship and the wind turbine support structure. In addition, simulation cases with an offset between the ship's plane of symmetry and the monopile axis showed a new form of damage to the ship's plating. During a head-on sliding collision, extensive plate tearing can occur due to its cutting at the deck line and concertina tearing under the pressure of the monopile. As a result, the hull may open over a large area, including the threat of unsealing the ship's collision bulkhead. The S355 grade steel can significantly reduce collision damage by up to 50% (from 20.6 m^2 to 10.5 m^2 for the case studied here).

1. Introduction

In response to the demand for more renewable energy, the number of offshore wind farms and ships operating in their immediate vicinity is growing. The energy power generated by a single turbine has significantly increased, and consequently, the size of its support structure has grown (Sánchez et al., 2019). The risk of severe consequences due to collisions is highly relevant for coastal areas. Overall statistical data on marine accidents in the years 2011–2020 indicated that collision, contact and grounding accidents represent 28%, 13% and 24%, respectively, giving a total of 65% of all marine accidents (Japan Transport Safety Board, 2020), as can be seen in Fig. 1. This represents about 563 accidents on average per year, often resulting in severe economic and environmental consequences. In recent years at least three severe accidents were reported. In 2021 the offshore wind installer Teras Fortress 2 capsized and almost sank after colliding with the monopile transition piece off the coast of southern China's sea (Wingrove, 2021; Yihe, 2021). The second was the collision of a monopile structure and substation platform by the drifting bulk carrier Julietta D, shortly after colliding at the anchorage area with the tanker Pechora Star in January 2022 (Buitendijk, 2022). The third was the collision of the cargo ship Petra L, most probably with the 6 m diameter monopile of the Gode Wind 1 in the North Sea, resulting in extensive hull damage (Fig. 2). It is too early to draw any conclusions as the collision occurred in April 2023, and the investigation is ongoing. With the increasing size and number of offshore installations, the risk of collision with ships rises. In many cases, neither the ship nor the monopile resistance to collision is sufficient, and there is growing interest in research on that.

The design of new ships follows the latest environmental protection regulations on gas emissions. Considerable progress has been made by introducing novel hull forms to reduce ship resistance (Lee et al., 2017; Yang and Kim, 2017; Yu et al., 2017; Niklas and Pruszko, 2019). Another way to improve the ship's energy efficiency is to reduce structural weight. This can be achieved using high-strength steel or composite material as an alternative for the ship hull design (Garbatov and Georgiev, 2022; Palomba et al., 2021). The sandwich type of structure is a standard solution for weight-saving and provides excellent crashworthiness, good damping properties and an economical solution (Palomba et al., 2022; Garbatov and Palomba, 2023). After the COVID-19 pandemic, steel prices rose significantly, and steel fabrication costs increased even more. In addition to the difficulty in assessing long-term economic and ecological impact, the potential to improve the structure's

* Corresponding author.
E-mail address: karol.niklas@pg.edu.pl (K. Niklas).

https://doi.org/10.1016/j.oceaneng.2023.115899
Received 30 June 2023; Received in revised form 18 September 2023; Accepted 20 September 2023
Available online 23 September 2023

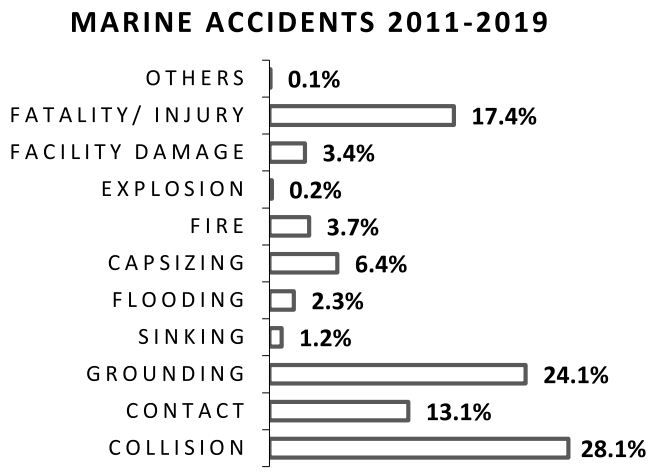

Fig. 1. Marine accidents by type between years 2011–2019 (Japan Transport Safety Board, 2020).

safety in case of a collision is an essential factor that may justify the use of high-strength steel. The selection of steel for hull construction is of great importance.

In recent years, collisions between ships and offshore support structures have gained considerable attention and have been the subject of numerous scientific studies. The collision consequence for three Offshore Wind Turbine (OWT) support structures was analysed in (Biehl, 2005), where the modelling assumptions were discussed. The Finite Element (FE) simulation of collision between a ship and a monopile structures was analysed in (Ren and Ou, 2009). Also, a new conceptual sphere device was presented to reduce wind turbine damage. The 3 MW wind turbine and 2000 displacement class ship were assumed at the time. The FE simulation between a ship and an offshore structure was analysed in (Bela et al., 2015). Different collision scenarios were studied to identify the sensitivity of the monopile to various parameters, including the impact of a velocity, nacelle mass, wind direction, soil stiffness, the vertical location of the impact point and wind orientation. The application of a crashworthy device consisting of a rubber blanket and outer shell to protect a monopile was presented in (Liu et al., 2015). The study presented in (Bela et al., 2017) aimed to analyse the crushing behaviour and the nacelle dynamics of a monopile having a diameter of 4.3 m when impacted by a ship. The simulation cases included parameters like ship impact velocity and location, wind direction, soil stiffness and deformability of the striking ship. It was found that the impact velocity significantly influences the OWT damage identifying three types of impact responses. The comparison of the anti-impact performance to the monopile, tripod and jacket foundations of the OWT was analysed in (Hao and Liu, 2017). The jacket was found to generate the minimum collision force, damage area and nacelle acceleration for the head-on impact cases. It was concluded that the jacket structure has the optimum comprehensive anti-impact performance under low-energy collisions among the three.

The study presented in (Yu and Amdahl, 2018a, 2018b) focused on the collision resistance of tubular offshore structures. The collision resistance between the 5 MW monopile OWT and vessel of 2000-tonne displacement, including detailed structural modelling of the groted connection, has been analysed (Mo et al., 2018). The authors found that even low-velocity impact may lead to significant failure of the grouted connection. The anti-collision performance of the fenders made of four different materials was investigated in (Han et al., 2019) and considered the case of a head-on collision between a ship and the tripod support structure. Jia et al., 2020 analysed the load on a 4 MW offshore wind turbine during the collision with a maintenance vessel. Moreover, the structural response to different environmental loads was carried out. The ultimate loads caused by storm surges were analysed in (Niklas, 2017). The development of practical modelling techniques for the collision analysis between a fixed-type offshore platform and an offshore supply vessel was investigated in (Mujeeb-Ahmed et al., 2020). The sensitivity analysis was conducted for different collision parameters to develop the simulation approach for analysed cases. Moreover, in recent years collision and grounding simulations of ships have used similar numerical approaches, i.e. (Yamada et al., 2008; Niklas and Kozak, 2016; Liu et al., 2018; Ringsberg et al., 2018).

Fig. 2. Collision damage of the ship Petra L. (LOA = 74m) on the Gode Wind 1 offshore wind farm (monopiles D = 6m, 6 MW) (Mandra, 2023).

The state of the art shows that ship collisions with offshore structures are a very timely topic. However, the previous research was primarily focused on turbines of up to 5 MW (diameter up to 5 m) and ships up to 2500 tonne displacement. Meanwhile, the offshore wind industry is developing rapidly. Nowadays, 10 MW wind turbines are installed, and the collision analysis needs to consider 5000 to 7000-tonne displacement Offshore Supply Vessels. In this respect, this study considers upgraded data according to the industry's needs. In contrast to the previous works, the presented study focuses on the ship's strength and not only the supporting structure. It also considers the modern shape of the ship's hull with a B-bow type, which has not been evaluated before. Notably, the size and weight of superstructures have increased so significantly in recent years that the crashworthiness of ships may be more critical than the superstructure itself. The article first analyses the case of a head-on central collision according to the DNV standards. The results demonstrate representative consequences of the collision for a modern Service Operation Vessel (6500-tonne displacement) and a large-sized 15 MW wind turbine (monopile diameter of 10 m). A frontal collision is chosen because the ship has the highest kinetic energy and the possible extensive hull damage over a wide area. However, other cases, such as side or rear-end collisions, can also be dangerous but are not discussed here. A head-on collision is of particular interest from the standpoint of ship safety. It is expected that during the sliding of the hull over a large monopile, a new form of damage may occur, that is, the tearing of the outer ship plating under the pressure of a monopile. The simulation of a head-on collision with an offset between the ship's PS and the monopile's axis of symmetry was used to analyse that.

The study's primary goal is to investigate the effect of changing the ship's material on the tearing of the hull plating caused by a head-on sliding collision with a monopile. The impact of the selection vessel's steel grade of S235, S355, and S460 (DNV, 2021e) on collision damage is performed. The ship's hull damage is compared with the use of internal energy, accounting for erosion, crushing force and the area of the hull opening. An important novelty in the present study is also a more detailed modelling of the transition part of the monopile, namely the grouted connection. At the transition piece, the design consists of a steel-concrete-steel sandwich structure with much greater local and zone stiffness and resistance to collision than a single plate used in most previous studies. Another essential aspect included here is the Soil-Structure stiffness Interaction (SSI) and deformability of both colliding objects – the ship and monopile. The effect of other loads like wind turbine, wind, waves, and currents are addressed in a simplified generalised manner.

2. Numerical simulation of the collision between a ship and an OWT monopile

The study was conducted using a non-linear FEM simulation performed by LS-dyna software v.11.2.0. The case of a head-on collision between a ship and an OWT monopile structure was analysed. The initial kinetic energy of the ship was primarily dissipated as plastic deformations of the colliding monopile and the vessel itself.

2.1. The ship and the monopile selected for the study

This analysis selected the modern 6500-tonne displacement Service Operation Vessel (SOV) with the innovative B-bow hull form. This shape was designed to have improved seakeeping performance on rough seas. The conical bow shape may have also not revealed a new beneficial feature – increased ability to slide over the monopile during a head-on impact. The primary vessel data is summarised in Table 1, and the reference plate thicknesses are shown in Fig. 3. The plate thickness of the D-deck, C-Deck, Stringer, Tank-Top is t = 7 mm, B-Deck has t = 15 mm and A-Deck, Main-Deck and Tween-Deck has t = 8 mm. The girder on the ship's Center Line (CL) is T600x10x150x15. The stiffeners at D-Deck are T220 × 8 × 100x8, and at C-Deck are T220x10x100x10. Girders are

Table 1
B-bow SOV particulars.

Service Operation Vessel (SOV)	
Type	B - bulbous bow
Length overall	83,70 m
Breadth	17,60 m
Depth to the main deck	10,70 m
Scantling draught	6,50 m
Deadweight DWT	2500 t
Displacement Δ	6480 t
Water (added mass)	324 t
Inertia moment I_{xx_COG}	2.82e8 kg m^2
Inertia moment $I_{yy\_COG} = I_{zz\_COG}$	2.06e9 kg m^2
COG from FP, WL	−41.3, 0, 0.3 m

T425 × 8 × 100x8. At B-Deck, stiffeners are T180x10x100x10, and girders are T425x12x150x15. At A-Deck, stiffeners are T160x10x100x10, and girders are T425x12x150 × 15mm. At the Main-Deck, Tween-Deck, there is a stringer T350x12x100x10. At the Tank Top, the plate thickness is t = 12 mm. The notations of decks are shown in Fig. 3.

According to the new NREL design, the monopile was selected as the modern support structure for wind turbines with a power of 15 MW (Gaertner et al., 2020). The basic data of the turbine and the monopile structure is summarised in Table 2. The detailed dimensions of the monopile are described in Table 3. The transition piece has a sandwich structure of steel-grout-steel, a plate thickness of 43 mm, and a grout layer thickness of 120 mm. This monopile design reflects the minimum structural design requirement for the generic U.S. East Coast site with a water depth of 30 m, wind speed described by a Weibull distribution with a mean velocity of 8.65 m/s and a shape parameter of 2.12. the corresponding significant wave height is 1.4 m, with a peak spectral period of 7.9 s. Notably, many of the actual wind farm locations exceed these environmental conditions. Thus, it was decided that the design having three times the thickness of the NREL plate thicknesses will be included in the analysis. The increased thickness is a reasonable assumption for large-sized 15 MW turbines dedicated mainly to deeper waters. This modified design at the transition piece has a plate thickness of 129 mm and a grout layer thickness of 120 mm. The material S355 was assumed for the monopile as the most used and preferred by the industry for manufacturing purposes. The production capacity for plate thicknesses currently reaches 320 mm and is being expanded.

2.2. Collision scenarios

The collision scenarios from 1 to 6 were defined according to the design standards (DNV, 2021f; DNV, 2021d) and recommended practice (DNV, 2021b). Additionally, the simulation cases with the offset between the ship's plane of symmetry and the monopile axis were included with similar remaining modelling assumptions to address the research questions. The special notation was used to identify specific load cases (Table 4). A similar notation is used in Chapter 4, presenting a more detailed description of the analysed collision scenarios and discussing the most important results. Many possible design load cases were limited to the proposed research program to show the most important findings. It is worth noticing that, from the ship's point of view, it is possible to define both more critical collision cases and much less critical ones. The selected simulation cases also include the influence of turbine thrust and torque. The monopile's environmental loads, such as wind, waves and current, were deliberately omitted as their impact on the analysed phenomena is much smaller. At the same time, the effect of ship movement due to waves, current and steering was considered in a simplified generalised way, as initial v_y (sway) and v_{rx} (roll) velocities. The combined effect on the ship was captured with minimal simulation cases. All the simulation cases are summarised in Table 5.

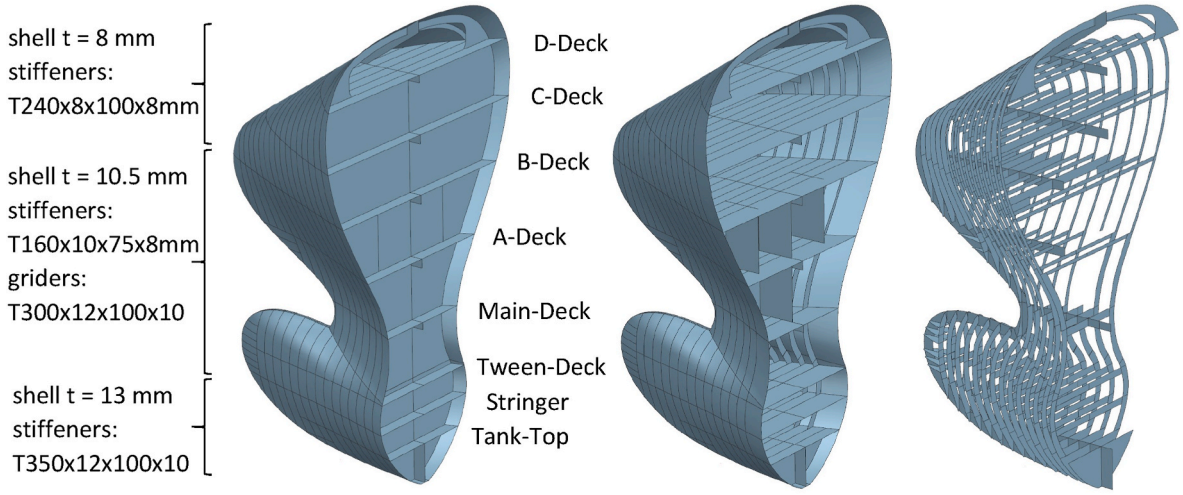

Fig. 3. Reference plating thickness of the ship structure.

Table 2
Descriptors of IEA Wind 15 MW turbine and monopile (Gaertner et al., 2020).

Large size monopile	
Power rating	15 MW
Turbine class	IEC Class 1B
Number of blades	3
Rotor diameter	240 m
Max generator torque	20 MNm
Max rotor thrust	2.8 MN
Nacelle total mass	821 t
Nacell moment of inertia I_{xx}	12.6E6 kg m^2
Nacell moment of inertia I_{yy}	21.4E6 kg m^2
Nacell moment of inertia I_{zz}	18.7E6 kg m^2
Nacell COG, tower top downwind	5.49, 0, 3.98
Hub height	150 m
Water depth (mean sea level)	30 m
Monopile embedment depth	45 m
Transition piece height	15 m
Monopile base diameter	10 m
Tower mass	860 t
Monopile mass	1318 tonne

Table 3
Detailed dimensions of monopile structure (Gaertner et al., 2020).

Location	Height [m]	Outer diameter [m]	Thickness [mm]
Monopile start	−75	10.000	55.341
Mud line	−30	10.000	55.341
−29.999		10.000	55.341
−25.000		10.000	55.341
−24.999		10.000	53.449
−20.000		10.000	53.449
−19.999		10.000	51.509
−15.000		10.000	51.509
−14.999		10.000	49.527
−10.000		10.000	49.527
−9.999		10.000	47.517
−5.000		10.000	47.517
−4.999		10.000	45.517
Water line	0	10.000	45.517
0.001		10.000	43.527
5.000		10.000	43.527
5.001		10.000	42.242
10.000		10.000	42.242
10.001		10.000	41.058
Tower start	15	10.000	41.058
15.001		10.000	39.496
28.000		10.000	39.496
28.001		10.000	36.456
41.000		9.926	36.456
41.001		9.926	33.779
54.000		9.443	33.779
54.001		9.443	32.192
67.000		8.833	32.192
67.001		8.833	30.708
80.000		8.151	30.708
80.001		8.151	29.101
93.000		7.390	29.101
93.001		7.390	27.213
106.000		6.909	27.213
106.001		6.909	24.009
119.000		6.748	24.009
119.001		6.748	20.826
132.000		6.572	20.826
132.001		6.572	23.998
Tower top	144.582	6.500	23.998

2.3. FE model

The finite element computational model for the conducted simulations was built in Ls-Dyna software and is shown in Fig. 4. The vessel structure was represented by the shell elements (fully integrated type 16) and the beam elements (Belytschko-Schwer) for the stiffener flanges. The size of finite elements was equal to 100 mm, which enabled a very detailed representation of outer plating, decks, bulkheads, walls, frames, stiffeners and brackets – Fig. 5. The bow section was modelled directly by shell and beam representations. The remaining part of the ship was modelled by the mass element at the ship's centre of gravity (COG) connected with the fore section by rigid beams. The added mass of water was also included as 5% of the ship's displacement. The vessel data is presented in Table 1. The FE model of the bow section consisted of a total number of 126E3 elements and 121E3 nodes. The monopile plating structure was modelled by the shell elements (fully integrated shell type 16). The grout was modelled by solid elements (fully integrated quadratic 8-node elements with nodal rotations). The element size at the transition piece was 100 mm, increasing gradually to 500 mm at the monopile end. The grout layer was modelled by the element size of 100 mm and three elements through the layer thickness. The contact between the grout and the monopile and between the grout and the transition piece was modelled by the algorithm AUTOMATIC_SURFACE_TO_SURFACE. This penalty-based contact algorithm is recommended for FE analysis of the grouted connection in (DNV, 2021a). The static and dynamic friction coefficient was 0.7. At the top of the tower, the mass element representing the nacelle centre point of gravity and inertia moments was placed and connected with the tower by rigid beams. The rotor thrust force and generator torque moment were assigned at the node. The downwind load case was assumed to be

Table 4
Notations.

Name	Description
Ship235_10532_180	
235	235 – the Yield point of the steel grade of the entire ship bow section.
1	Plate thicknesses of the monopile. One means plate thicknesses acc. to NREL design; 3 means three times the thicknesses acc. to NREL design.
0	The offset between the ship's PS and the vertical z-axis of the monopile. 0 means the offset equal 0 m. 2 means the offset equals 2.5 m. 5 means the offset equal 5 m.
5	Initial velocity of the ship in the x-axis direction (v_x). 2 means 2.572 m/s (5 knots). 3 means 3.858 m/s (7.5 knots). 5 means 5.144 m/s (10 knots). 6 means 6.43 m/s (12.5 knots). 7 means 7.716 m/s (15 knots).
3	Initial velocity of the ship in y-axis direction (v_y). 1 means 1 m/s (1.94 knots). 2 means 2 m/s (3.9 knots). 3 means 3 m/s (5.83 knots)
2	Initial rotational velocity over the x-axis direction (v_{rx}). 1 measns 0.1 rad/s (5.7 deg/s). 2 means 0.2 rad/s (11.5 deg/s). Ratotialnal velocity is oriented towards the monopile.
180	Optional suffix describing the direction of the thrust force. The 000 means direction downwind. The 090 indicates the side case in the y-axis direction. The 180 means upwind direction.

in a positive x-axis direction. The detailed data of the wind turbine are presented in Table 2. The soil structure interaction was modelled according to the API standard (American Petroleum Institute, 2014) and implemented in the DNV recommended practice (DNV, 2021c). The non-linear p-y springs were placed in the x-axis and y-axis direction at a vertical distance of 1 m. The load-deflection (p-y) curves for sand were calculated with parameters presented in Table 6.

Additionally, for the simplification purposes of the model, the boundary condition of $d_z = 0$ was assigned at the bottom end of the monopile. Various other values of bottom stiffness can occur depending on the location and are determined each time based on geological studies of the seabed. The influence of modelling the Soil-Structure Interaction (SSI) on the collision response of a monopile was analysed in (Samsonovs et al., 2014). The authors concluded that the effect of the SSI for collision at 5 m/s was minor, whereas for the velocity of 2 m/s disregarding the elasticity of the foundation leads to substantial overestimation of plastic deformations of the OWT. In studies devoted to jacket-type foundations, the effect of SSI is mostly omitted due to little impact on the structure response during the collision (Le Sourne et al., 2015). Also, the study presented in (Yu and Amdahl, 2018a) concluded that the pile-soil modelling can be simplified using pinned boundary conditions at the mud line. However, for the simulations of large-diameter monopile structures, the inclusion of the SSI is essential because assuming fixed boundary conditions at the mudline may lead to an overestimation of the damage of the collided structure (Bela et al., 2017). This also affects the damage to the stricken ship, and therefore consideration of the SSI effect is necessary and has been included in this study.

Moreover, analysing SSI's impact, the above publications assumed a non-deformable ship. The model under discussion assumes simulations of the deformable monopile and ship type, which is a more realistic case. However, studying the effect of ground stiffness is beyond the present study objectives. The monopile model consisted of 135E3 shell elements, 144E3 solid elements and 231E3 nodes.

The initial velocity was assigned to all parts of the vessel. The contact between the ship and column was modelled using AUTOMATIC_SURFACE_TO_SURFACE algorithm. The connection between the internal ship structure and internal monopile structure was modelled using AUTOMATIC_SINGLE_ SURFACE algorithm. The static and dynamic friction coefficient was equal to 0.2 in this contact definition.

The material properties of steel were assumed according to the (DNV, 2022). The density of steel was 7850 [kg/m^3], the Young modulus was 210 GPa, and the Poisson ratio was 0.3. The true stress-strain curve was modelled as a combination of stepwise linear and a power law with a yield plateau - Fig. 6. The values of specific points depend on the steel grade and the plate thickness defined in the design recommendations. The calculated material curves for the ship are presented in Fig. 7. The primary principal strain failure criterion EPSMAJ was applied. The failure strain of steel was assumed according to Eqn (1) (Lehmann and Peschmann, 2002), with the uniform strain $\varepsilon_g = 0.02$ and the necking

Table 5
Collision simulation cases.

Number	Notation	Reference to the research questions
1	Ship235_10200	What are the consequences of the head-on collision between the ship and the wind turbine according to the DNV design rules?
2	Ship235_10500	
3	Ship235_10700	
4	Ship235_30200	
5	Ship235_30500	
6	Ship235_30700	
7	Ship235_35200	Is the head-on collision case covered by the design regulations of the monopile also a safety-critical case for the ship?
8	Ship235_35300	
9	Ship235_35500	
10	Ship235_35600	
11	Ship235_35700	
12	Ship355_35200	Can changing the material of the vessel improve collision safety?
13	Ship355_35300	
14	Ship355_35500	
15	Ship355_35600	
16	Ship355_35700	
17	Ship460_35200	
18	Ship460_35300	
19	Ship460_35500	
20	Ship460_35600	
21	Ship460_35700	
22	Ship235_35511	Variants to include ship's v_y, v_{rx}, rotor thrust force and torque moment.
23	Ship235_35522	
24	Ship235_10300_000	
25	Ship235_10300_180	

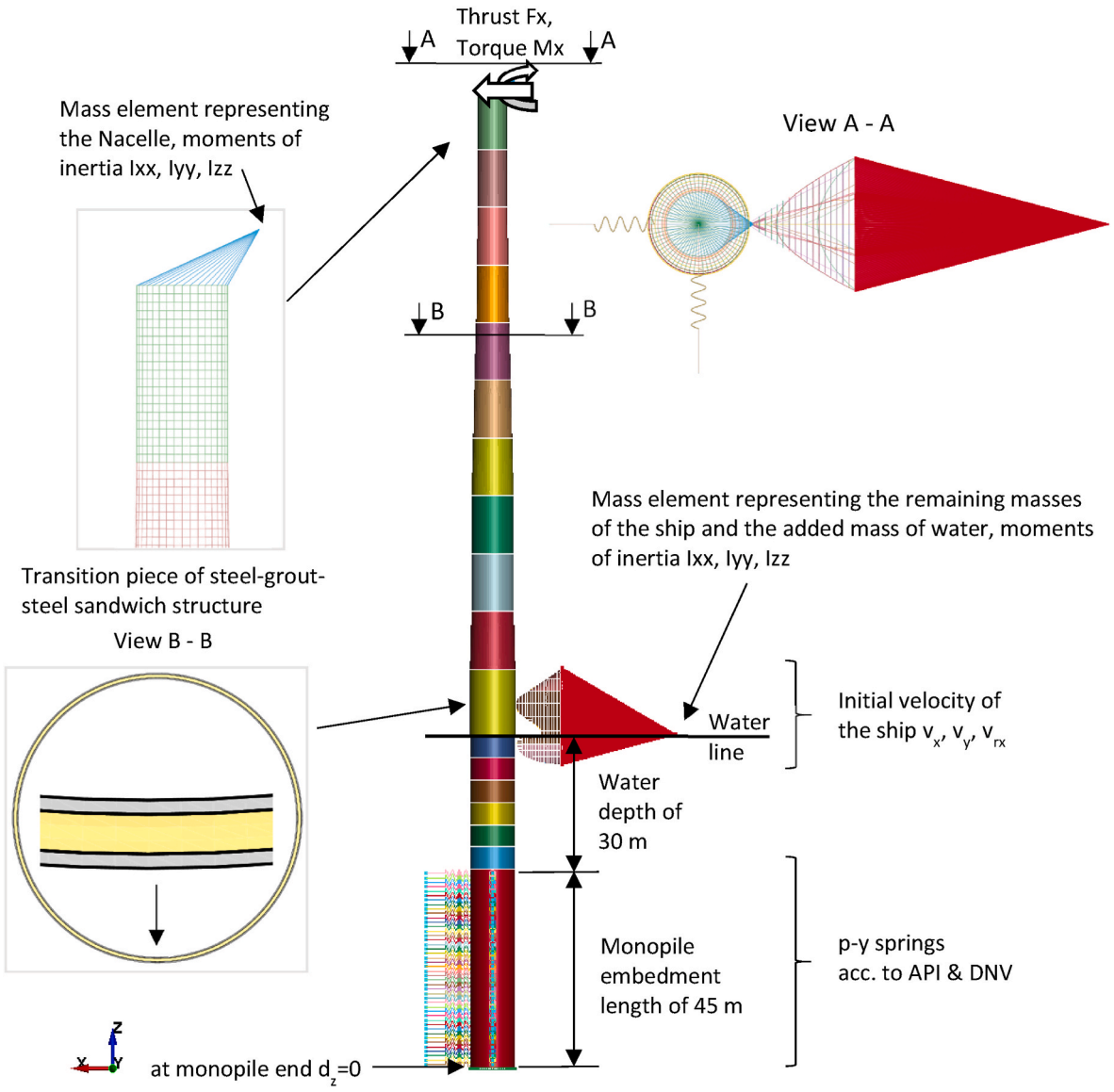

Fig. 4. FE model of the ship (SOV, 6500 tonn displacement) colliding monopile (Ø10 m, 15 MW turbine).

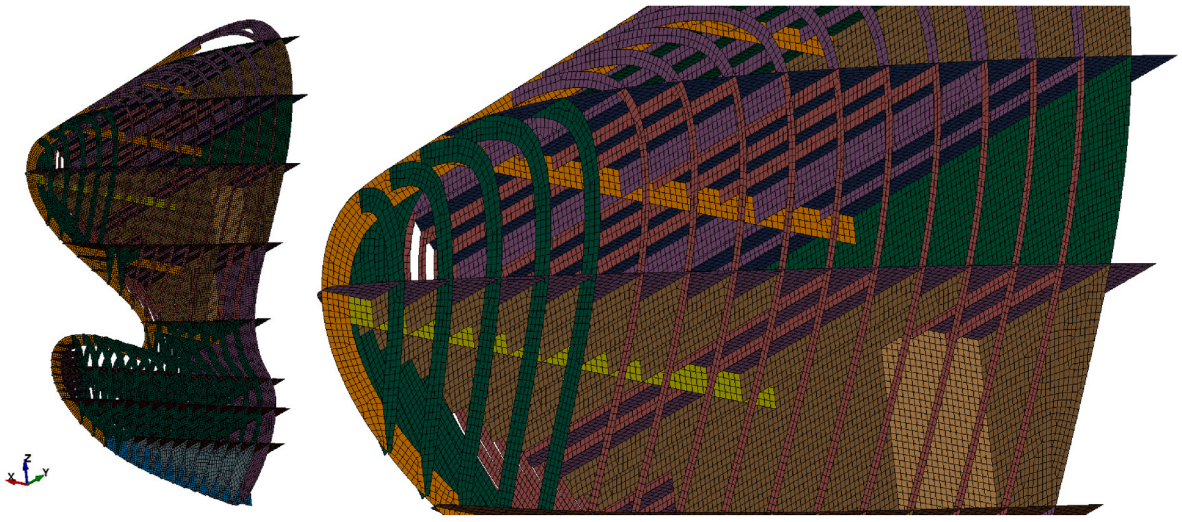

Fig. 5. Sample detailed FE mesh of the ship, element size of 100 mm, outer plating is hidden.

Table 6
Ground properties.

Parameter	Value	Unit
Angle of internal friction of sand φ′	36	deg
Initial modulus of subgrade reaction	24439	kN/m3
Coefficient C1	3.2	-
Coefficient C2	3.6	-
Coefficient C3	60	-
Unit weight – saturated	20	kN/m^3
Unit weight – effective γ	10.2	kN/m^3

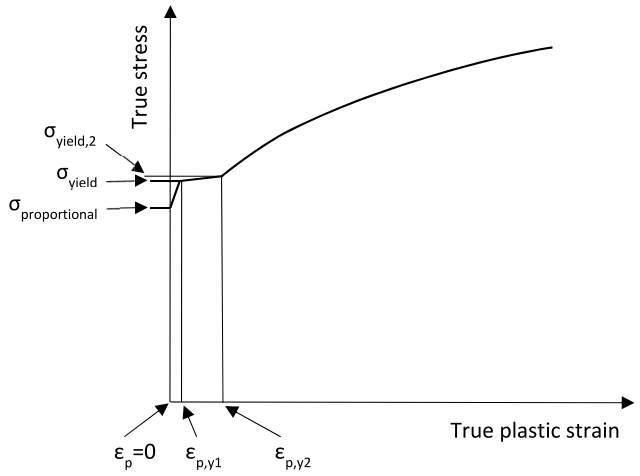

Fig. 6. True stress-strain curve (DNV, 2021e).

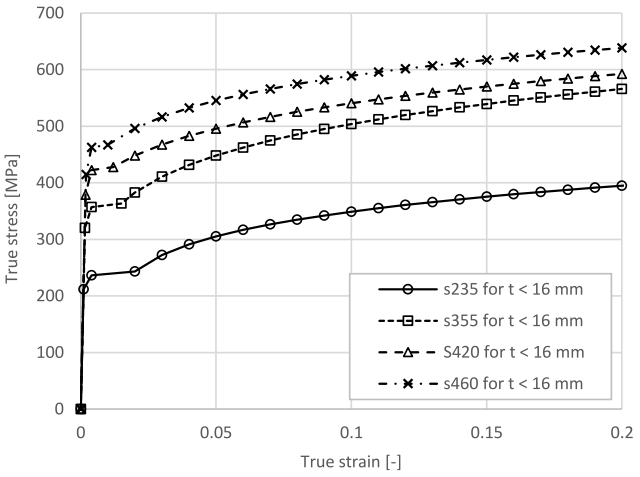

Fig. 7. Calculated true stress-strain curves for steel structure of the ship.

strain $\varepsilon_e = 0.65$ according to DNV (2021b). The material model was implemented by the MAT123_MODIFIED_PIECEWISE_LINEAR card. Since it's a very influential parameter, it's worth noticing that different failure criteria may be found in other research works devoted, i.e. to the comparison of various bottom and side structures (Naar et al., 2002), analysing the effect of rebounding during ship-ship collision (Rio Prabowo et al., 2017), benchmarking the scaled collision experiment (Ringsberg et al., 2018), criterium based on averaging various experiments (Liu, et al., 2017), benchmarking failure criteria (Calle et al., 2017) and analysing fixed-type offshore platforms (Mujeeb-Ahmed et al., 2020). The failure model used in this study can be the average compared to the beforementioned. The sensitivity study of material relations on ship structure damage was presented in (Ehlers, 2010). The influence of selected strain-based failure criteria was presented in (Niklas and Bera, 2022). The strain-rate effect of steel was modelled according to the Cowper-Symonds (Cowper and Symonds, 1957) – Eqn (2), (Paik et al., 2017) and the parameters are shown in Table 7. The sensitivity study on the work hardening and strain-rate effects was presented in (Storheim and Amdahl, 2017).

$$\varepsilon_f(l_e) = \varepsilon_g + \varepsilon_e\left(\frac{t}{l_e}\right) \tag{1}$$

where:

ε_f – failure strain,
ε_g – uniform strain,
ε_e – necking strain,
t – plate thickness,
l_e – length of a single element.

$$\frac{\sigma_d}{\sigma_s} = 1 + \left(\frac{\dot{\varepsilon}}{C}\right)^{\frac{1}{p}} \tag{2}$$

where:

σ_d – dynamic yield stress
σ_s – static yield stress
$\dot{\varepsilon}$ - strain rate,
C, p – constants of Cowper–Symonds relation

The grout material, characterised as ultra-high strength concrete, was modelled according to the material model validated in (Mo et al., 2018). The material model MAT_CONCRETE_DAMAGE_REL3 (MAT72_R3) implemented in the LS-dyna was used. The data of ultra-performance grout Ducorit® S1 determined by the manufacturer were applied, as presented in Table 8. Compressive and tensile strength characteristic values were used to calculate the in-situ values according to the design standard (DNV, 2021f). The compressive strength equal to 89.8 MPa, and the tensile strength of 3.1 MPa was used as the simulation input data. The dynamic increase factor (DIF) included the strain-rate effect according to the Comité euro-international du béton (2010). The erosion of the grout was modelled by the numerical erosion algorithm MAT_ADD_EROSION and the criterium of the maximum principal strain of 0.1.

The finite element mesh convergence analysis was performed and confirmed adequate representation using an element size of 100 mm at the collision zone – Fig. 8. The comment on the computation performance shall be included here. The simulation time for a single collision simulation case takes about 15 days and 10 h on a standard PC workstation (on 4-cores, CPU gen. 2020). Thus, from a practical point of view, using supercomputer power, the presented research was possible in a reasonable time. For comparison, the simulation on 24 cores took about 40 h. Linear scalability of computing performance was evaluated up to 96 cores (4 nodes, Linux, CPU gen. 2015).

3. Results and discussion

The head-on collision of a modern SOV with the large monopile substructure is represented by cases 1 through 6. These cases assume the

Table 7
Parameters used to define strain rate.

Material	C (s^{-1})	p	
S235	40.4	5	(Cowper, G. R. Symonds, 1957)
S355	3,200	5	(Paik, Kim, Lee, Jung, & Kim, 2017)
S420	3,200	5	
S460	3,200	5	

Table 8
The material properties of grout Ducorit® S1 (ITW Performance Polymers, 2018).

Property	Value	Unit
Compressive strength f_c (char./in-situ)	110/89.8	MPa
Static modulus of elasticity E_c	35	GPa
Dynamic modulus of elasticity E_d	35	GPa
Tensile strength f_t (char./in-situ)	5/3.1	MPa
Density ρ	2250	kg/m^3
Poisson ratio υ	0.19	-
Strength enhancement	DIF (CDIF & TDIF)	
Failure principle strain	0.1	-

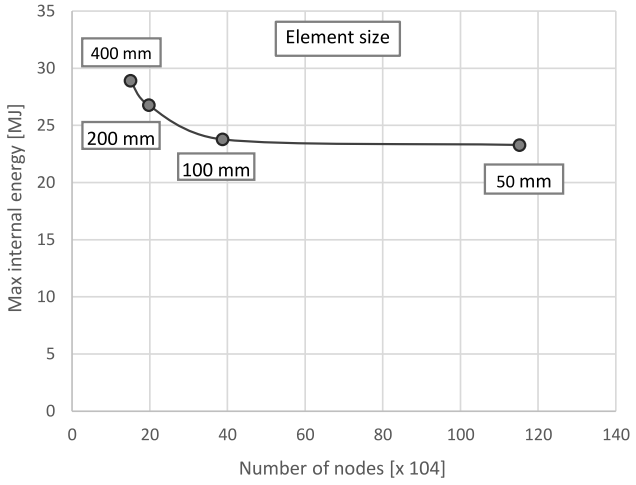

Fig. 8. Mesh convergence analysis.

ship moves in the x-axis direction at initial speeds of 5, 10 and 15 knots. Cases 1 through 3 reflect a collision with the monopile having plate thicknesses assumed according to the NREL design and denoted here as 1. This monopile design assumes very low environmental loads and has relatively thin plates with an outer diameter of 10 m, equal to 55 mm at the base and 21 mm at the top of the tower. Subsequent cases 4 through 6 reflect similar collision cases but with increased plate thickness labelled 3 to represent the stiff structure needed for more demanding operational wind park sites. All these cases were configured following the DNV-RP standards for assessing the monopile accidental collision impact. The calculated collision damage results represent two extreme forms of damage for a head-on collision between a ship and a large-diameter (10 m) monopile. The mode of extensive plastic deformations of the monopile was observed in cases 1 to 3 - Fig. 9. The energy of the collision is absorbed mainly by the transition piece of the monopile, and the ship damage is very low for all the analysed velocities – Fig. 10. The left part of Fig. 10 shows the results for the monopile and the right part for the ship. Both graphs share the x-axis of time. The grouted connection has been completely damaged. The steel-concrete-steel sandwich structure, under the impact of the ship collapses very deeply. However, it was found that the inner and outer pipe section is responsible for about 50% of the energy absorbed by the monopile (Fig. 10). The concrete layer itself absorbs very little energy, while the outer and inner pipe dents and wedges. The opposite mode of extensive ship damage was observed for cases 4 through 6, in which the ship absorbs most of the impact energy - Figs. 11 and 12. The monopile structure is slightly locally dented. The internal energy of the monopile is relatively very low, and the grouted section is still responsible for capturing about half of it - Fig. 12.

The resultant collision force is presented in Figs. 13 and 14. The value of the maximum crashing force of 38 MN is quite similar for cases from 1 to 3 (the monopile is relatively prone to local indentations) and cases from 4 to 6 (the monopile is relatively stiff to local indentations). However, the nature of the course of structural failure is different. For cases from 1 to 3 in which local collapse of the pipe occurs, the force gradient is noticeably smaller than for cases from 4 to 6 in which the reasonably stiff structure of the ship's bow section folds. This is also reflected in the values of maximum acceleration at the centre of gravity of the nacelle and ship – Fig. 15. The maximum resultant acceleration at the centre of gravity (COG) of the nacelle equals 12.4 m/s^2. It takes place for simulation case 6. Accordingly, the ship's COG is 5.9 m/s^2 for case 3. For cases 1 through 6, the overall consequence of the collision is much more severe for a wind turbine that collapses by indentation at ship speeds of about 7.5 knots and above. This corresponds to an initial kinetic energy of 5 MJ. It is important to note that for all of the above design cases, the critical safety of the vessel is not compromised.

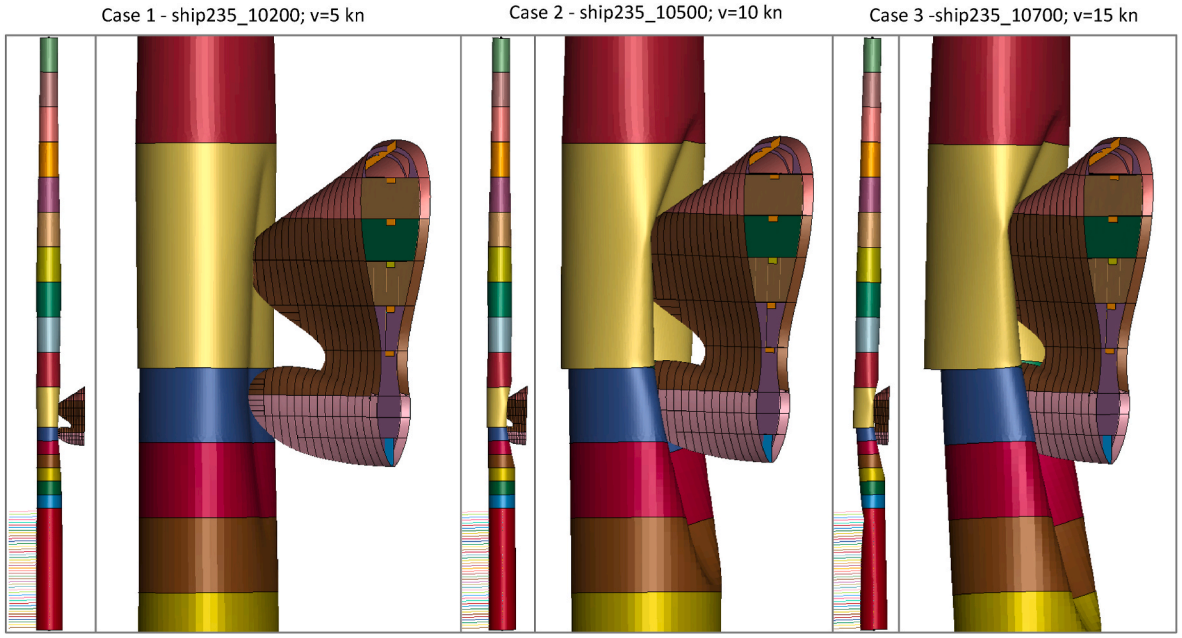

Fig. 9. The damage form of extensive plastic deformations of the monopile (cases 1 to 3).

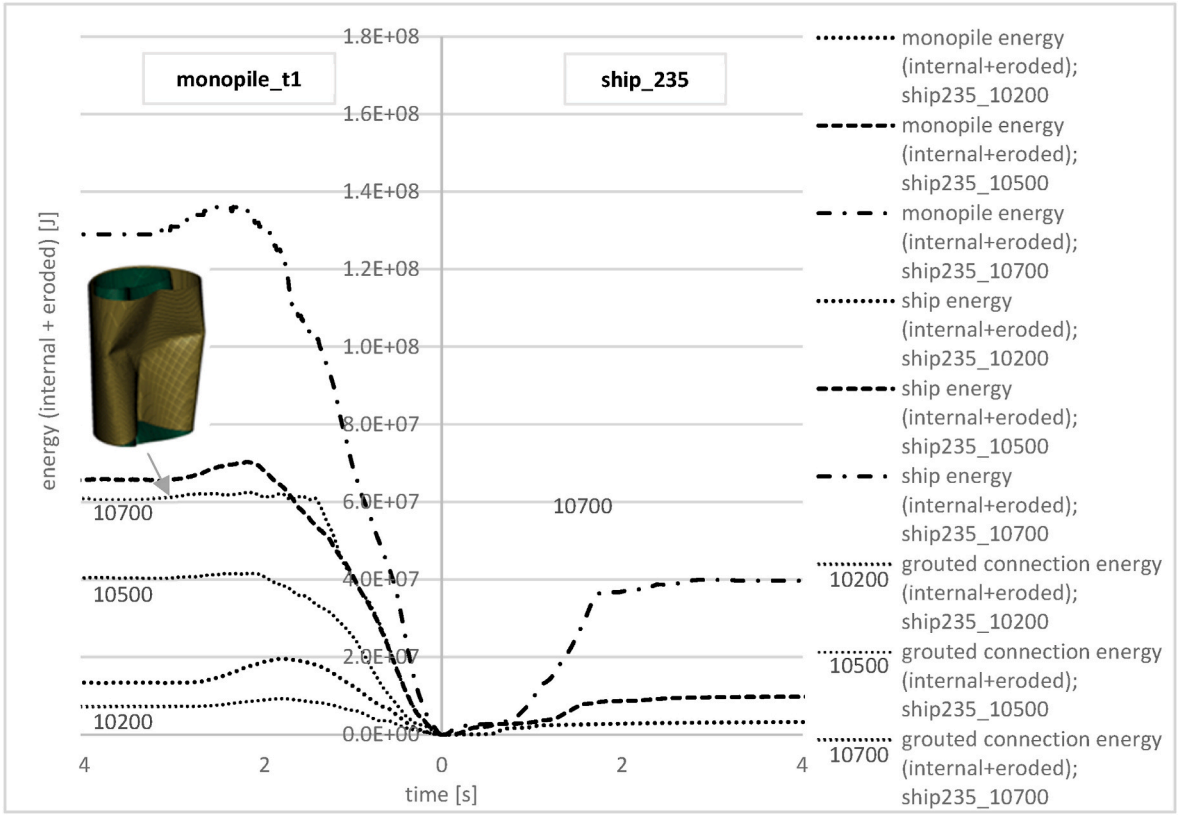

Fig. 10. Energy dissipation between the monopile and ship (cases 1 to 3).

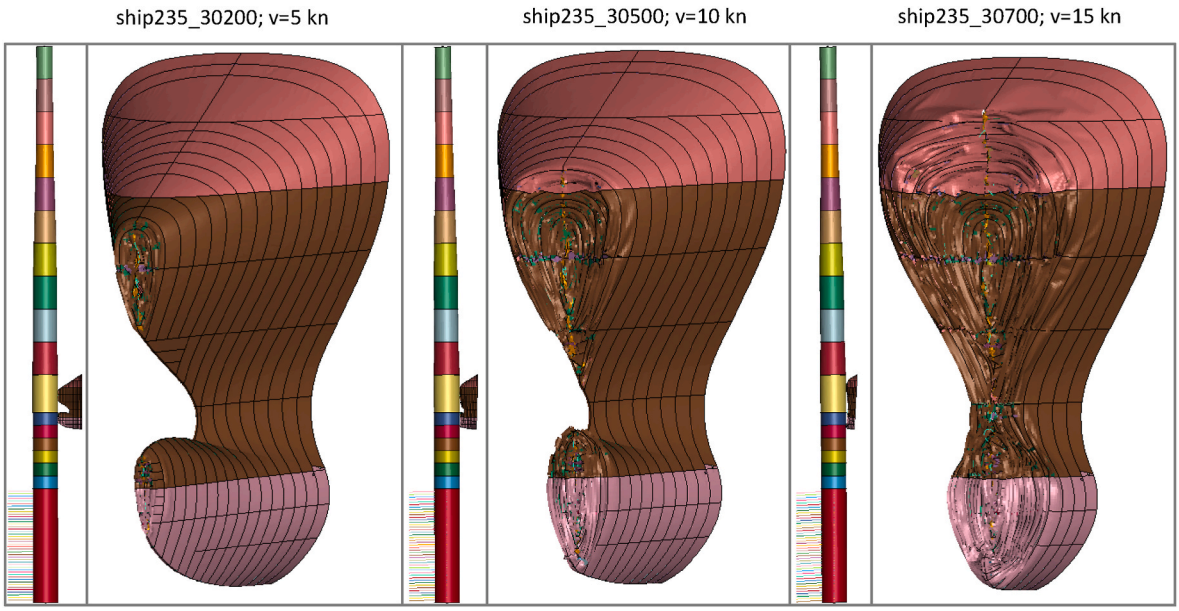

Fig. 11. Damage form of extensive plastic deformations of the ship's bow (cases 4 to 6).

Extensive damage to the bow section affects a compartment separated from the rest of the ship by a watertight collision bulkhead.

However, is the frontal collision case covered by the design rules of the wind turbine also a safety-critical case for the ship? The ship's bow is usually considered a relatively stiff and resistant section. As demonstrated above, the ship structure could capture a large amount of impact energy by extensive plastic deformation and even folding the entire bow section. At the same time, it does not need to be necessarily the worst-case scenario. It is expected that a new form of damage may occur during the sliding of the hull's outer surface over a large monopile. That is, cutting and tearing the outer hull plating under the pressure of a monopile. Large-size monopiles have tremendous stiffness and, at the same time, an oval shape that facilitates hull sliding. The ship's outer plating can potentially be torn along a significant length. To investigate this form of destruction, head-on collision simulations were modified to account for the offset between the ship's plane of symmetry and the

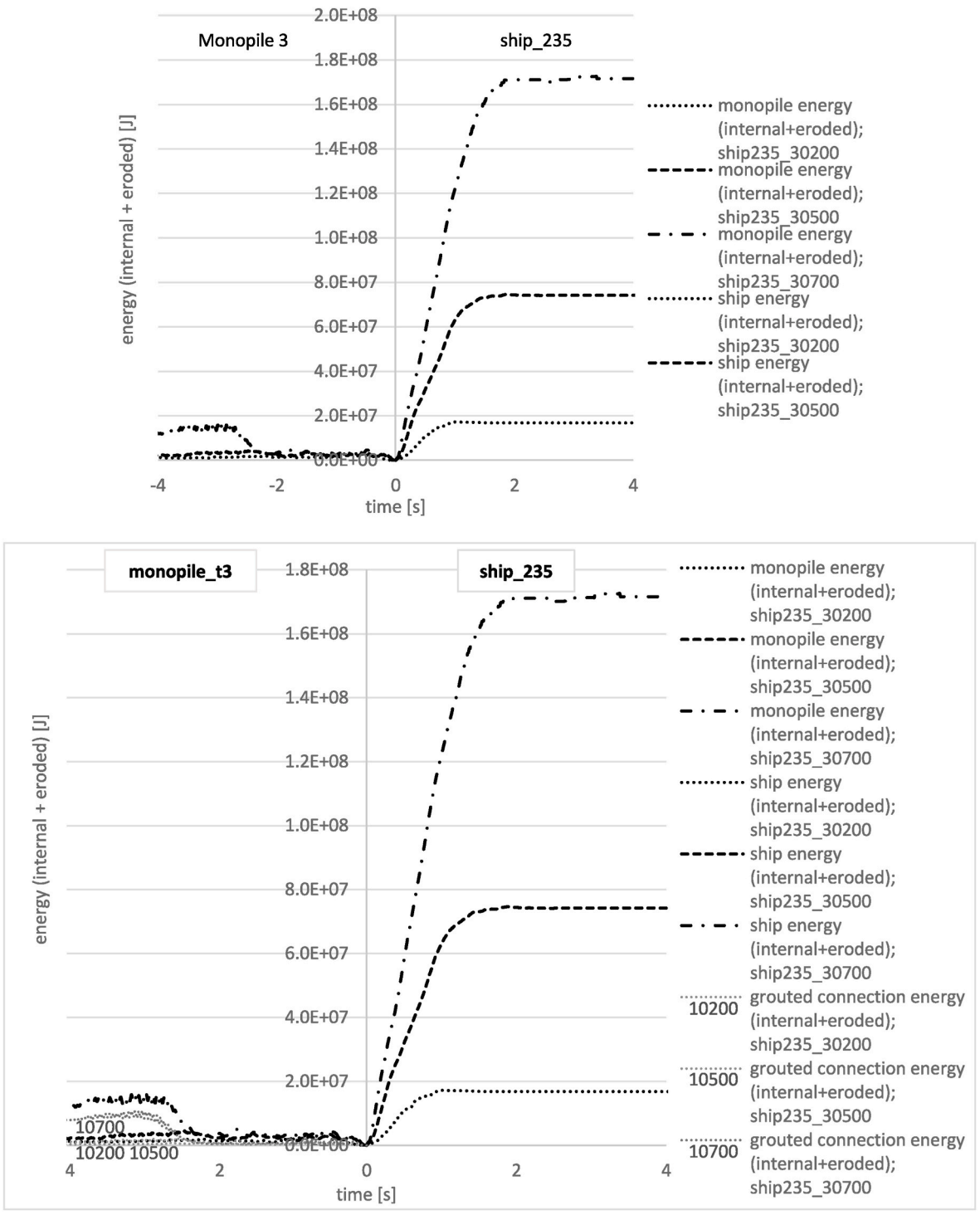

Fig. 12. Energy dissipation between the monopile and the ship (cases 4 to 6).

monopile's vertical axis. This allows the ship's hull to move forward along the stricken monopile. Simulation cases 7, 9 and 11 are presented to analyse this hull damage, which refers to the offset value of 5 m and the ship's forward speed of 5 knots, 10 knots and 15 knots, accordingly. Severe hull damage was observed in the form of a large opening of the hull plating – Fig. 16. The outer plating was cut and torn by pressure from the monopile resulting in damage much more critical from the ship's safety point of view than observed in cases 1 to 6. The critical unsealing damage was observed on the collision bulkhead for the speed of 15 knots - Fig. 16. The area of hull opening was equal to 1.5 m^2, 20.6 m^2 and 51.8 m^2 for the initial vessel speed of 5 knots, 10 knots and 15 knots, accordingly.

The following question arises - how to reduce the opening of the outer plating cost-effectively? Can changing the material of the vessel improve collision safety? To answer this question, the following results show the effect of the vessel's steel grade on collision damage. In these simulation cases, a similar offset of 5 m was assumed between a ship and monopile symmetry axes that allow the ship to slide over the monopile during a frontal impact. Fig. 17 shows the strong dependence of the effect of a ship's steel grade on the outer hull plating rapture. The steel grades of S355 and S460 have higher Yield points, and the failure strain provides significantly higher collision safety for the presented

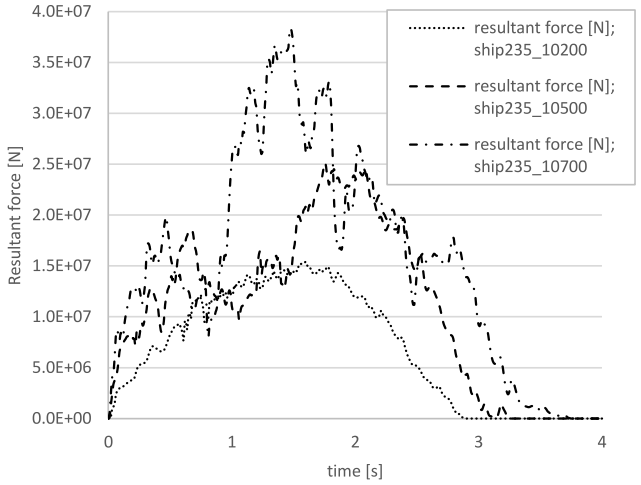

Fig. 13. Resultant collision force (cases 1 to 3).

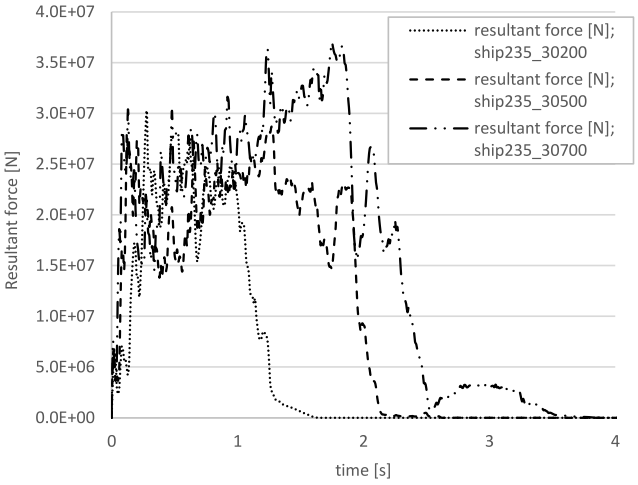

Fig. 14. Resultant collision force (cases 4 to 6).

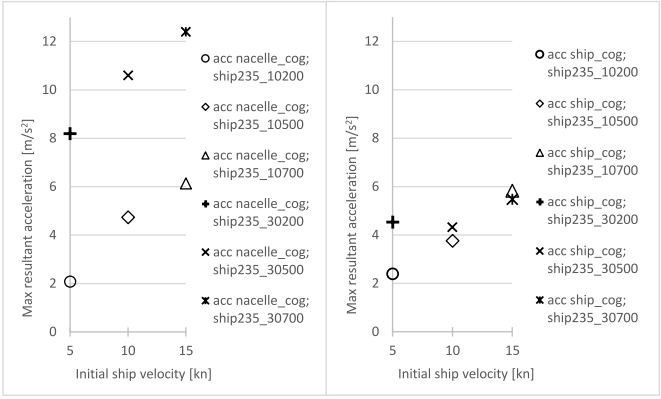

Fig. 15. Maximum resultant accelerations of the nacelle's cog and the ship's cog.

simulation cases. It is also essential to notice the influence of the ship's initial energy (velocity) on the ability of the ship structure to utilise improved material properties. For a small vessel speed of 5 knots, the small impact of the material was observed, and the overall hull damage was low. For the medium speed of 10 knots, the highest effect of the material properties was observed. The area of hull rapture drops by as much as 50% (from 20.6 m^2 to 10.5 m^2) using material S355 instead of normal strength steel S235. For the S460, the reduction of damage is equal to 64%. The possible effect on rising collision safety is significant. For the high ship speed of 15 knots, the utilisation of material properties drops due to the overall capacity of the structure to absorb collision energy. For the steel S355, the reduction of hull opening was 22%, and for the S460, it was 31%. For all materials, the damage to the entire impacted side of the ship's bow section is extensive – bottom row in Fig. 20. An additional search for an increase in collision strength can be directed toward design changes that include geometry modifications. However, it can be observed that for the steel grades of S355 and above, the critical damages of the collision bulkhead are less severe than for the S235. Further, more comprehensive research is needed to analyse it in more detail.

The simulation cases from 22 to 24, including thrust force and torque moment from the rotor, transverse linear velocity v_y, and angular velocity r_{vx} in the analysis, affected the ship and monopile-a damage results. For example, the transverse velocity components of speed v_y and rotational velocity v_{rx} act in a direction pushing the colliding vessel towards the monopile. It caused an increase in hull damage as can be seen in Fig. 19. On the other hand, if the additional velocities act in the opposite direction, the damage is lower. Overall it's worth noting that even though many collision cases were analysed in this article, it's only a fracture of countless possible scenarios. It is worth realising that from both the ship's and the monopile's point of view, and it is possible to define more critical cases of a collision simulation. Thus, it was decided that the article presents only the crucial results significant for answering the above research questions and enabling the achievement of the article's objective in the most possible compensated and generalised manner.

Considering the practical application of a material for a ship's hull, it is worth estimating the increase in the cost. In the beginning, however, it should be noted that the capital expenditure, including material, labour, energy and other factors, are changing with time, which means that the estimate may change significantly over time. The assumed values are relevant to central-eastern Europe and are not supported by published data. Moreover, the assumptions follow the data of the OSV vessel analysed in this article. The average cost of steel S235 was assumed as $800/tonn. The S355 and S460 steel were assumed to be 35% and 46% more expensive, respectively. Next, a reduction factor in the weight of the steel structure due to the use of higher-strength material was assumed to be 15% for S355 steel and 20% for S460 steel. Next, manufacturing costs were assumed as 150% of the material cost for S235 steel. For S355 steel, the cost was assumed to be higher by 10%, and for S460 steel by 20%. The resulting bare steel hull production costs assume a combined 10% value of other costs (including margin). For such assumptions and a bare hull weight of 1700 tonnes, the production cost is about $3.7 M$. The estimated cost of a bare hull is about 20% of the total cost of a ship worth about 19 M$. Thus, the evaluated hull production cost increased by 12% for S355 steel and 20% for S460 steel. At the same time, by rough estimates, the total cost of the ship increased by about 2.5% for S355 steel and about 4% for S460. The large potential of rising collision safety versus the estimates of impact on the ship cost is shown in Fig. 18.

4. Conclusions

The offshore wind energy sector is growing exponentially. By the end of this decade, the already installed capacity is expected to increase 7-fold. Today's monopile support structures reach a height of 240 m, a weight of 2000 tonnes, a diameter of 10 m and a plate thickness of 150 mm. By 2050 the offshore wind installations may increase 50 times compared to the current amount. Most structures will be installed close to the shore and directly to the shipping routes. The existing size, number and density of the offshore facilities are just the tip of the

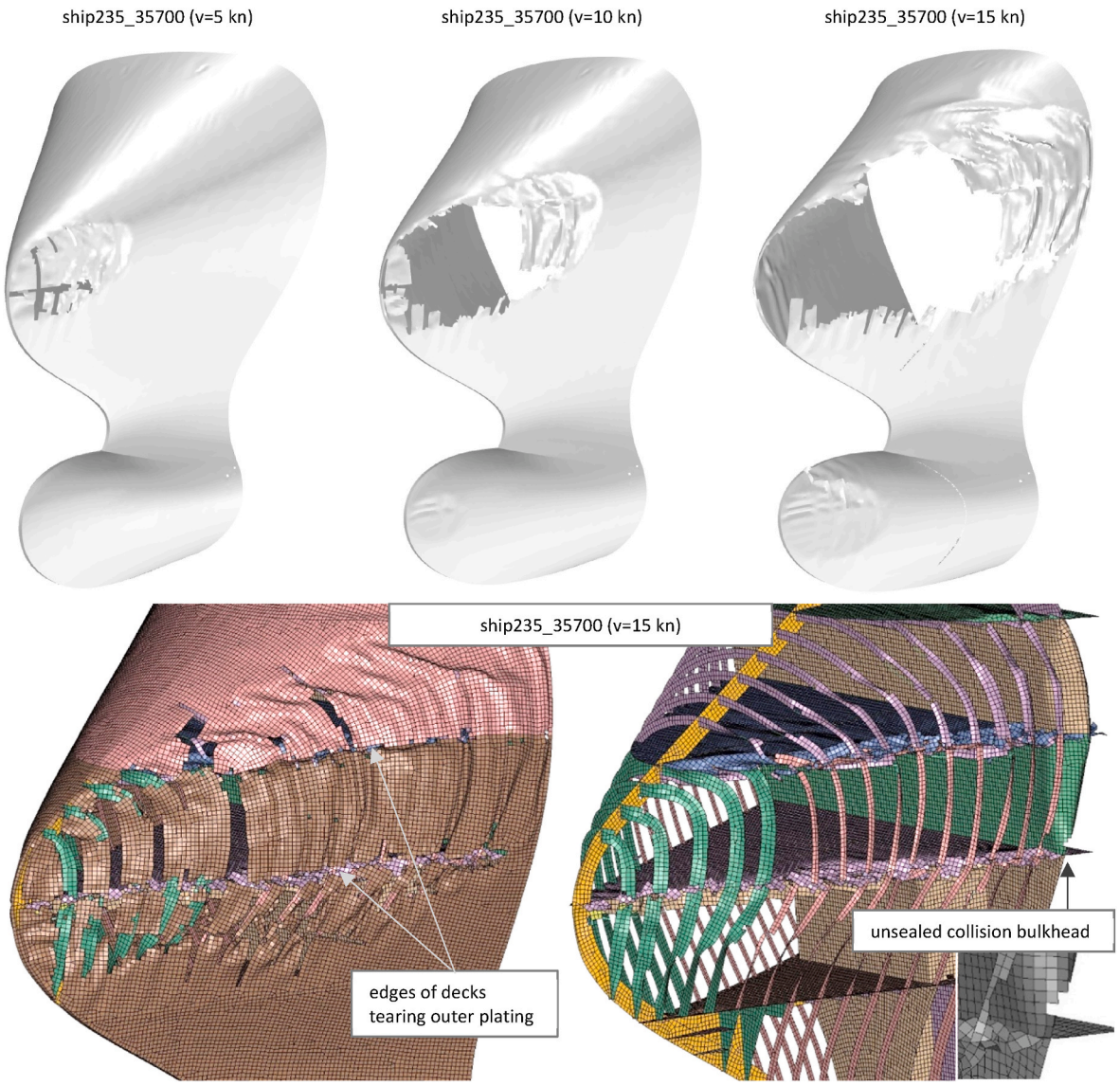

Fig. 16. Rapture of ship's outer plating. Upper left to right: cases 7, 9, 11. Below: Damage form of outer plating and internal structure, including collision bulkhead.

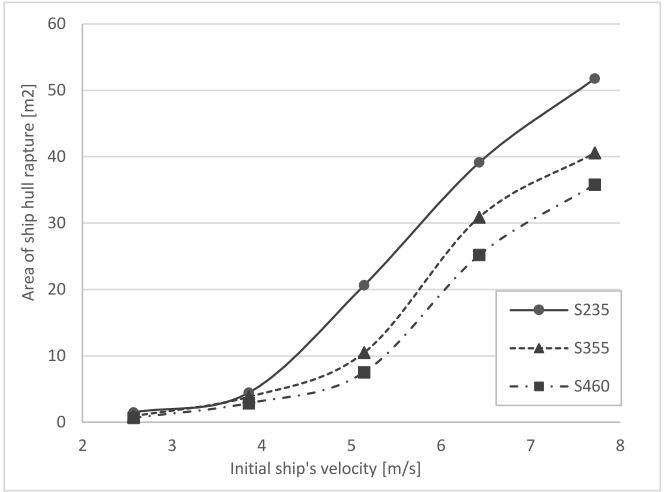

Fig. 17. Influence of ship's steel grade on rapture area of the outer plating.

iceberg to bring new challenges of providing sufficient safety for ships. This study analysed the head-on collision between 6500 tonnes displacement SOV and the 10 m diameter monopile as a case study that addresses current industry needs.

The consequences of the frontal collision between the modern SOV and the monopile of a 15 MW wind turbine calculated according to the present DNV design rules depend very much on the relative stiffness of the ship and the colliding structure. The collision energy dissipation is shared between the two colliding objects. Suppose the monopile is made of relatively thin metal plates (e.g., up to 50 mm with a base diameter of 10m). In that case, it will absorb most collision energy through extensive deformation in the impacted region. The tower's collapse meant indentation was possible even for a relatively low ship speed of 7.5 knots. The inclusion of detailed modelling of the grouted connection is essential. The inner and outer pipe of the grouted connection is responsible for about 50% of the internal energy absorbed by the monopile. The steel-concrete-steel sandwich structure demonstrated much higher collision resistance than a single-layer pipe. The opposite boundary scenario is a relatively stiff monopile which suffers minimal damage, and most of the ship's kinetic energy is converted into the plastic deformation energy of her structure. For the frontal collision case assumed here in which the ship's plane of symmetry lies in the axis of the

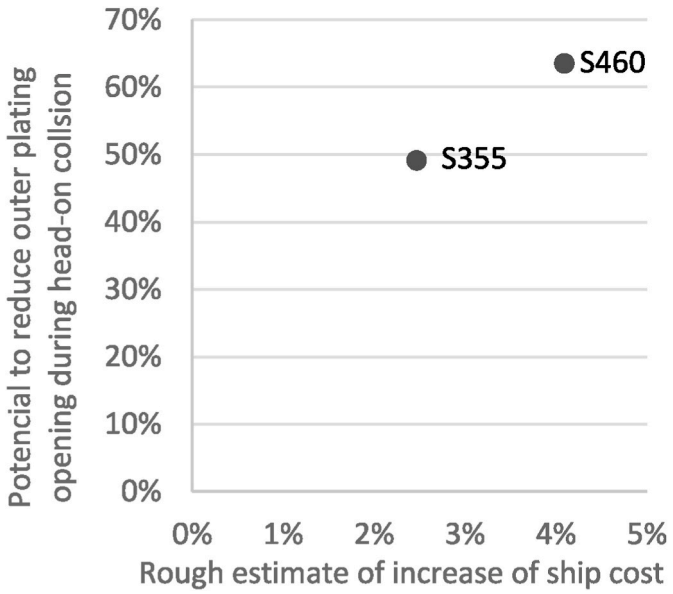

Fig. 18. Potential to reduce hull outer plating rapture vs impact on ship cost.

monopile, the critical safety of the ship related to its survival is not directly threatened. Even the extremely extensive bow section collapse is limited to the ship's compartment, separated from the rest by a watertight collision bulkhead.

The consequences of colliding with a large-size monopile for the ship can be extremely severe for the cases not assessed by the monopile design rules. The new destruction form of the hull was identified: the cutting and concertina tearing of the outer plating under the pressure of the monopile. This damage may occur in a head-on collision with an offset between the ship's PS and the monopile vertical axis. The sliding of the vessel over the monopile can take place at a long distance. The resulting damage to the hull's outer plate opening may be extensive. An unfavourable collision scenario can even potentially lead to unsealing the collision bulkhead. Large-sized monopiles near shipping routes can cause danger to SOV operating in wind parks and the rest of ships of various types and sizes. Some ship types, like the ro-ro, are particularly fragile because of stability and the limited presence of transverse bulkheads.

The collision resistance of the ship may be increased by applying the higher strength steel instead of standard grade S235. The most significant impact of material selection was seen for such a collision energy value that the structure can effectively absorb for reasons arising from its structural design. In contrast, the impact of the material is less visible for collisions of very low energy when the damage is minimal, as well as for very high energy when the damage exceeds the ability of the design to absorb it. For the analysed head-on sliding collision scenarios, the hull rapture area can be reduced by as much as 50% by applying the steel grade S355. This significant reduction of hull opening from 20 m^2 to 10 m^2 was observed for a vessel speed of 10 knots. The risk of unsealing the collision bulkhead was also reduced. Using high-strength steels like S460 does not bring a relatively proportional increase in collision strength.

CRediT authorship contribution statement

Karol Niklas: Conceptualization, Methodology, Investigation, Resources, Writing – original draft, Writing – review & editing, Visualization, Project administration, Funding acquisition. **Alicja Bera:** Investigation, Writing – review & editing. **Yordan Garbatov:** Supervision, Writing – review & editing.

Declaration of competing interest

The authors declare that they have no known competing financial interests or personal relationships that could have appeared to influence the work reported in this paper.

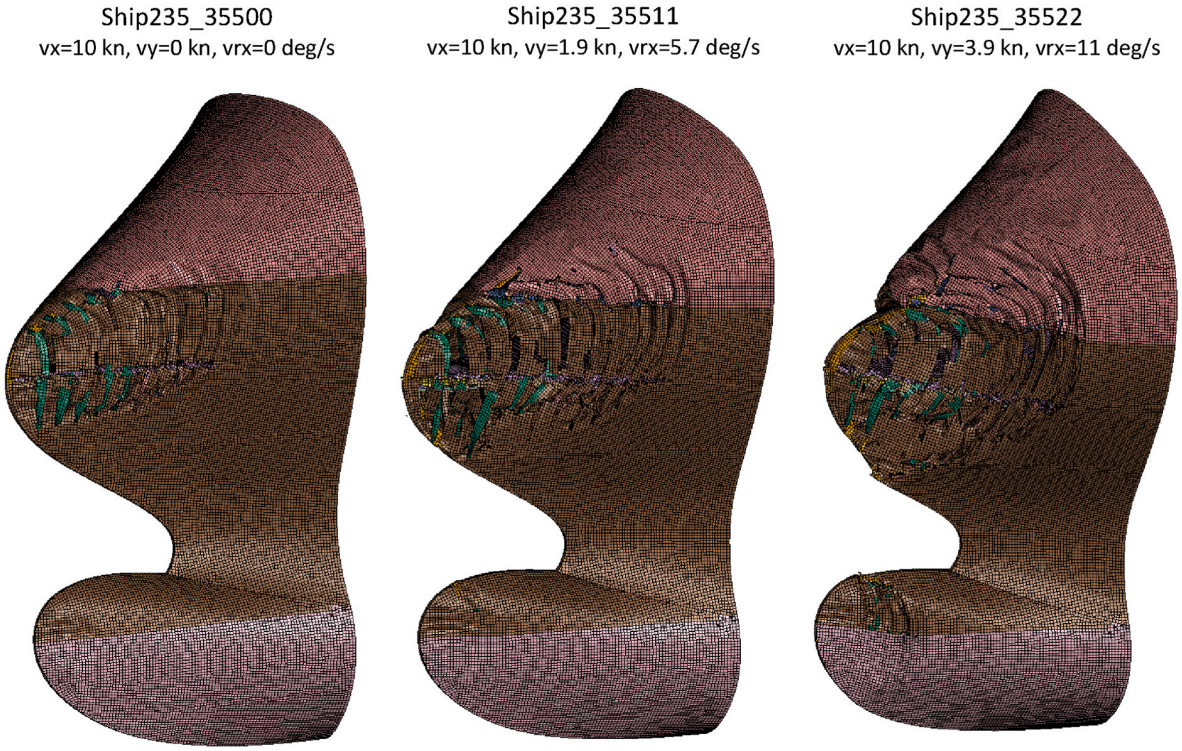

Fig. 19. Sample influence of ship's v_y, v_{rx} velocities on the hull damage. Left to right: cases 19, 22, 23.

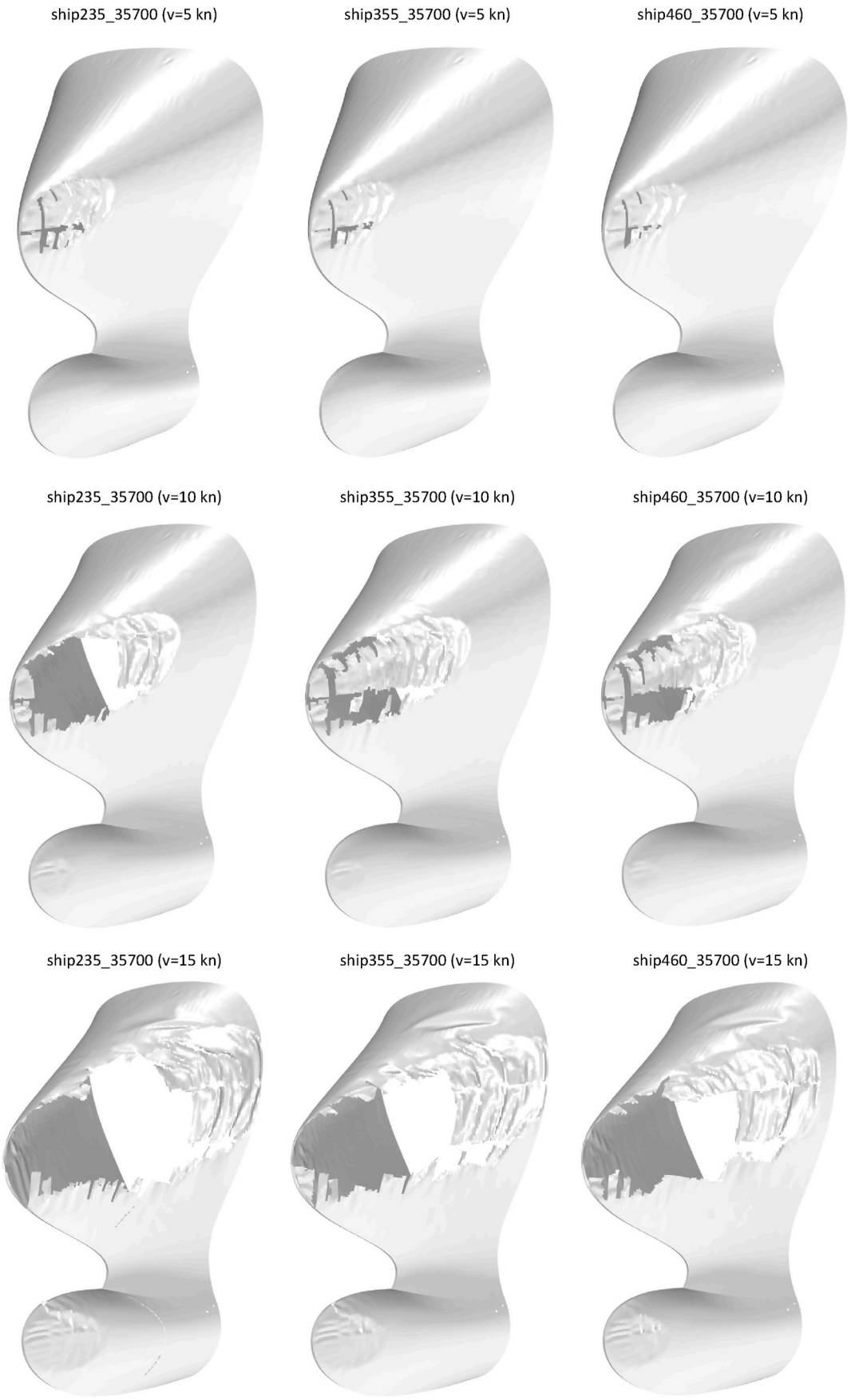

Fig. 20. Rapture of ship's outer plating.

Data availability

No data was used for the research described in the article.

Acknowledgements

Financial support for these studies is from the Gdańsk University of Technology by the DEC-02/2022/IDUB/II.1/AMERICIUM grant under the Americium - 'Excellence Initiative - Research University' program is gratefully acknowledged. This research was also supported by the Academic Computer Centre in Gdansk (CI TASK). The authors thank the reviewers for their valuable comments.

References

American Petroleum Institute, 2014. API Recommended Practice 2A-WSD Planning, Designing, and Constructing Fixed Offshore Platforms—Working Stress Design.

Bela, A., Buldgen, L., Rigo, P., Le Sourne, H., 2015. Numerical crashworthiness analysis of an offshore wind turbine monopile impacted by a ship. In: Analysis and Design of Marine Structures - Proceedings of the 5th International Conference on Marine Structures, MARSTRUCT 2015. https://doi.org/10.1201/b18179-87, 661–669.

Bela, A., Le Sourne, H., Buldgen, L., Rigo, P., 2017. Ship collision analysis on offshore wind turbine monopile foundations. Mar. Struct. 51, 220–241. https://doi.org/10.1016/j.marstruc.2016.10.009.

Biehl, F., 2005. Collision Safety Analysis of Offshore Wind Turbines. 4th LSDYNA European Conference, pp. 27–34.

Buitendijk, M., 2022. Julietta D Damages Wind Turbine Foundation, Master and Chief Officer under Suspicion. https://swzmaritime.nl/news/2022/02/03/julietta-d-damages-wind-turbine-foundation-master-and-chief-officer-under-suspicion/. (Accessed 18 September 2023).

Calle, M.A.G., Verleysen, P., Alves, M., 2017. Benchmark study of failure criteria for ship collision modelling using purpose-designed tensile specimen geometries. Mar. Struct. 53, 68–85. https://doi.org/10.1016/j.marstruc.2017.01.001.

Comité euro-international du béton, 2010. Model Code. First Complete Draft-Vol1, Lausanne (Switzerland).

Cowper, G.R., Symonds, P.S., 1957. In: Strain-hardening and Strain-Rate Effects in the Impact Loading of Cantilever Beams. https://doi.org/10.21236/ad0144762.

DNV, 2021a. DNV-RP-0419 - Analysis of Grouted Connections Using the Finite Element Method.

DNV, 2021b. DNV-RP-C204 - Structural Design against Accidental Loads.

DNV, 2021c. DNV-RP-C212 Offshore Soil Mechanics and Geotechnical Engineering.

DNV, 2021d. DNV-ST-0437 - Loads and Site Conditions for Wind Turbines.

DNV, 2021e. DNVGL-RP-C208 - Determination of Structural Capacity by Non-linear Finite Element Analysis Methods. September.

DNV, 2021f. DNVGL-ST-0126 - Support Structures for Wind Turbines.

DNV, 2022. DNV-RP-C208 Determination of Structural Capacity by Non-linear Finite Element Analysis Methods.

Ehlers, S., 2010. The influence of the material relation on the accuracy of collision simulations. Mar. Struct. 23 (4), 462–474. https://doi.org/10.1016/j.marstruc.2010.12.002.

Gaertner, E., Rinker, J., Sethuraman, L., Zahle, F., Anderson, B., Barter, G., Viselli, A., 2020. Iea Wind Offshore Reference Wind. Golden. https://www.nrel.gov/docs/fy20osti/75698.pdf. (Accessed 18 September 2023).

Garbatov, Y., Georgiev, P., 2022. Air pollution and economic impact from ships operating in the port of varna. Atmosphere 13 (9), 1526. https://doi.org/10.3390/atmos13091526.

Garbatov, Y., Palomba, G., 2023. Applied sciences risk-based hybrid lightweight ship structural design accounting for carbon footprint, 2023 Appl. Sci. 13 (6), 3583. https://doi.org/10.3390/app13063583.

Han, Z., Li, C., Deng, Y., Liu, J., 2019. The analysis of the anti-collision performance of the fender with offshore wind turbine tripod impacted by ship and the coefficient of restitution. Ocean Eng. 194, 106614 https://doi.org/10.1016/j.oceaneng.2019.106614.

Hao, E., Liu, C., 2017. Evaluation and comparison of anti-impact performance to offshore wind turbine foundations: monopile, tripod, and jacket. Ocean Eng. 130, 218–227. https://doi.org/10.1016/j.oceaneng.2016.12.008.

ITW Performance Polymers, 2018. In: Technical Data Sheet - DUCORIT®. Ultra-high Performance Grout. https://www.foundocean.com/Up/Comp/7188/13124963/13199998-KAGFHMTL/f/Ducorit S2.S5.S5r.pdf. (Accessed 18 September 2023).

Japan Transport Safety Board, 2020. In: Statistics of Marine Accidents. https://www.mlit.go.jp/jtsb/statistics_mar.html. (Accessed 18 September 2023).

Jia, H., Qin, S., Wang, R., Xue, Y., Fu, D., Wang, A., 2020. Ship collision impact on the structural load of an offshore wind turbine. Global Energy Interconnection 3 (1), 43–50. https://doi.org/10.1016/j.gloei.2020.03.009.

Le Sourne, H., Barrera, A., Maliakel, J.B., 2015. Numerical crashworthiness analysis of an offshore wind turbine jacket impacted by a ship. J. Mar. Sci. Technol. 23 (5), 694–704. https://doi.org/10.6119/JMST-015-0529-1.

Lee, J., Park, D.M., Kim, Y., 2017. Experimental investigation on the added resistance of modified KVLCC2 hull forms with different bow shapes, 2. In: Proceedings of the Institution of Mechanical Engineers Part M: Journal of Engineering for the Maritime Environment, 231. https://doi.org/10.1177/1475090216643981, 395–410.

Lehmann, E., Peschmann, J., 2002. Energy absorption by the steel structure of ships in the event of collisions. Mar. Struct. 15 (4–5), 429–441. https://doi.org/10.1016/S0951-8339(02)00011-4.

Liu, B., Villavicencio, R., Zhang, S., Guedes Soares, C., 2017. A simple criterion to evaluate the rupture of materials in ship collision simulations. Mar. Struct. 54, 92–111. https://doi.org/10.1016/j.marstruc.2017.03.006.

Liu, Bin, Pedersen, P.T., Zhu, L., Zhang, S., 2018. Review of experiments and calculation procedures for ship collision and grounding damage. Mar. Struct. 59, 105–121. https://doi.org/10.1016/j.marstruc.2018.01.008.

Liu, C., Hao, E., Zhang, S., 2015. Optimisation and application of a crashworthy device for the monopile offshore wind turbine against ship impact. Appl. Ocean Res. 51, 129–137. https://doi.org/10.1016/j.apor.2015.03.004.

Mandra, J.O., 2023. Article in Offshore-energy.biz. https://www.offshore-energy.biz/cargo-ship-strikes-orsteds-gode-wind-1-offshore-wind-farm-suffers-massive-damage/. (Accessed 18 September 2023).

Mo, R., Li, M., Kang, H., 2018. Transient behaviour of grouted connections of offshore wind turbines subject to ship impact. Appl. Ocean Res. 76, 159–173. https://doi.org/10.1016/j.apor.2018.05.006.

Mujeeb-Ahmed, M.P., Ince, S.T., Paik, J.K., 2020. Computational models for the structural crashworthiness analysis of a fixed-type offshore platform in collisions with an offshore supply vessel. Thin-Walled Struct. 154, 106868 https://doi.org/10.1016/j.tws.2020.106868.

Naar, H., Kujala, P., Simonsen, B.C., Ludolphy, H., 2002. Comparison of the crashworthiness of various bottom and side structures. Mar. Struct. 15 (4–5), 443–460. https://doi.org/10.1016/S0951-8339(02)00012-6.

Niklas, K., Kozak, J., 2016. Experimental investigation of Steel-Concrete-Polymer composite barrier for the ship internal tank construction. Ocean Eng. 111 https://doi.org/10.1016/j.oceaneng.2015.11.030.

Niklas, K., Pruszko, H., 2019. Full-scale CFD seakeeping simulations for case study ship redesigned from V-shaped bulbous bow to X-bow hull form. Appl. Ocean Res. 89, 188–201. https://doi.org/10.1016/j.apor.2019.05.011.

Niklas, K., 2017. Strength analysis of a large-size supporting structure for an offshore wind turbine. Pol. Marit. Res. 24, 156–165. https://doi.org/10.1515/pomr-2017-0034.

Niklas, K., Bera, A., 2022. The influence of selected strain-based failure criteria on ship structure damage resulting from a collision with an offshore wind turbine monopile. Pol. Marit. Res. 28 (4), 42–52. https://doi.org/10.2478/pomr-2021-0048.

Paik, J.K., Kim, K.J., Lee, J.H., Jung, B.G., Kim, S.J., 2017. Test database of the mechanical properties of mild, high-tensile and stainless steel and aluminium alloy associated with cold temperatures and strain rates. Ships Offshore Struct. 12, S230–S256. https://doi.org/10.1080/17445302.2016.1262729.

Palomba, G., Crupi, V., Garbatov, Y., 2021. Environmental impact of lightweight structures in marine applications. In: Developments in the Analysis and Design of Marine Structures. CRC Press.

Palomba, Giulia, Marchese, S.S., Crupi, V., 2022. Cost, energy efficiency and carbon footprint analysis of hybrid lightweight bulk carrier, 2022 J. Mar. Sci. Eng. 10 (7), 957. https://doi.org/10.3390/jmse10070957.

Ren, N., Ou, J., 2009. Dynamic numerical simulation for ship-OWT collision. In: Proceedings of 2009 8th International Conference on Reliability, Maintainability and Safety, ICRMS 2009. https://doi.org/10.1109/ICRMS.2009.5269985, 1003–1007.

Ringsberg, J.W., Amdahl, J., Chen, B.Q., Cho, S.-R., Ehlers, S., Hu, Z., Zhang, S., 2018. MARSTRUCT benchmark study on non-linear FE simulation of an experiment of an indenter impact with a ship side-shell structure. Mar. Struct. 59, 142–157. https://doi.org/10.1016/j.marstruc.2018.01.010.

Rio Prabowo, A., Myung Bae, D., Min Sohn, J., Fauzan Zakki, A., Cao, B., Hyung Cho, J., 2017. Effects of the rebounding of a striking ship on structural crashworthiness during ship-ship collision. Thin-Walled Struct. 115, 225–239. https://doi.org/10.1016/j.tws.2017.02.022.

Samsonovs, A., Giuliani, L., Zania, V., 2014. Soil structure interaction in offshore wind turbine collisions. In: Proceedings of the International Conference on Structural Dynamic, EURODYN, 2014-January(July), pp. 3651–3658.

Sánchez, S., López-Gutiérrez, J.S., Negro, V., Esteban, M.D., 2019. Foundations in offshore wind farms: evolution, characteristics and range of use. Analysis of main dimensional parameters in monopile foundations. J. Mar. Sci. Eng. 7 (12), 1–19. https://doi.org/10.3390/JMSE7120441.

Storheim, M., Amdahl, J., 2017. On the sensitivity to work hardening and strain-rate effects in non-linear FEM analysis of ship collisions. Ships Offshore Struct. 12 (1), 100–115. https://doi.org/10.1080/17445302.2015.1115181.

Wingrove, M., 2021. Salvage Required for Listing Chinese Offshore Lifeboat, Four Still Missing. https://www.rivieramm.com/news-content-hub/news-content-hub/salvage-required-for-listing-chinese-offshore-liftboatnbsp-66769. (Accessed 18 September 2023).

Yamada, Y., Endo, H., Pedersen, P.T., 2008. Effects of buffer bow structure in ship-ship collision. Int. J. Offshore Polar Eng. 18 (2), 133–141.

Yang, K.-K., Kim, Y., 2017. Numerical analysis of added resistance on blunt ships with different bow shapes in short waves. J. Mar. Sci. Technol. 22 (2), 245–258. https://doi.org/10.1007/s00773-016-0407-9.

Yihe, X., 2021. Search Continues for Missing Crew from Capsized Wind Installer Offshore China. Retrieved from. https://www.upstreamonline.com/energy-transition/search-continues-for-missing-crew-from-capsized-wind-installer-offshore-china/2-1-1045303.

Yu, J.-W., Lee, C.-M., Lee, I., Choi, J.-E., 2017. Bow hull-form optimisation in waves of a 66,000 DWT bulk carrier. Int. J. Nav. Archit. Ocean Eng. 9 (5), 499–508. https://doi.org/10.1016/J.IJNAOE.2017.01.006.

Yu, Z., Amdahl, J., 2018a. A review of structural responses and design of offshore tubular structures subjected to ship impacts. Ocean Eng. 154, 177–203. https://doi.org/10.1016/j.oceaneng.2018.02.009.

Yu, Z., Amdahl, J., 2018b. Analysis and design of offshore tubular members against ship impacts. Mar. Struct. 58, 109–135. https://doi.org/10.1016/j.marstruc.2017.11.004.